RESOURCE GEOLOGY

doi: 10.1111/j.1751-3928.2011.00182.x Resource Geology Vol. 62, No. 1: 99–118

Thematic Article

# Geology and Hydrothermal Alteration of the Duobuza Gold-Rich Porphyry Copper District in the Bangongco Metallogenetic Belt, Northwestern Tibet

Guangming Li,[1] Jinxiang Li,[1] Kezhang Qin,[1] Ji Duo,[2] Tianping Zhang,[3] Bo Xiao[1] and Junxing Zhao[1]

[1]*Key Laboratory of Mineral Resources, Institute of Geology and Geophysics, CAS, Beijing,* [2]*Tibet Bureau of Geology and Exploration, Lhasa, Tibet and* [3]*No. 5 Geological Party, Tibet Bureau of Geology and Exploration, Golmu, China*

**Abstract**

The Duobuza gold-rich porphyry copper district is located in the Bangongco metallogenetic belt in the Bangongco-Nujiang suture zone south of the Qiangtang terrane. Two main gold-rich porphyry copper deposits (Duobuza and Bolong) and an occurrence (135 Line) were discovered in the district. The porphyry-type mineralization is associated with three Early Cretaceous ore-bearing granodiorite porphyries at Duobuza, 135 Line and Bolong, and is hosted by volcanic and sedimentary rocks of the Middle Jurassic Yanshiping Formation and intermediate-acidic volcanic rocks of the Early Cretaceous Meiriqie Group. Simultaneous emplacement and isometric distribution of three ore-forming porphyries is explained as multi-centered mineralization generated from the same magma chamber. Intense hydrothermal alteration occurs in the porphyries and at the contact zone with wall rocks. Four main hypogene alteration zones are distinguished at Duobuza. Early-stage alteration is dominated by potassic alteration with extensive secondary biotite, K-feldspar and magnetite. The alteration zone includes dense magnetite and quartz-magnetite veinlets, in which Cu-Fe-bearing sulfides are present. Propylitic alteration occurs in the host basic volcanic rocks. Extensive chloritization-silicification with quartz-chalcopyrite or quartz-molybdenite veinlets superimposes on the potassic alteration. Final-stage argillic alteration overlaps on all the earlier alteration. This alteration stage is characterized by destruction of feldspar to form illite, dickite and kaolinite, with accompanying veinlets of quartz + chalcopyrite + pyrite and quartz + pyrite assemblages. Cu coexists with Au, which indicates their simultaneous precipitation. Mass balance calculations show that ore-forming elements are strongly enriched during the above-mentioned three alteration stages.

**Keywords:** Bangongco metallogenetic belt, Duobuza porphyry copper district, hydrothermal alteration, mass balance, mineralization, northwestern Tibet.

## 1. Introduction

The Duobuza gold-rich porphyry copper district is located in the Bangongco metallogenetic belt (BGCMB, Fig. 1) in Tibet and was discovered by No.5 Geological Team, Tibet Bureau of Geology and Exploration (TBGE) in 2000 (No.5 Geological Team, TBGE, 2003). Two main gold-rich porphyry copper deposits and an

Received 31 August 2010. Accepted for publication 15 October 2011.
Corresponding author: G. LI, Key Laboratory of Mineral Resources, Institute of Geology and Geophysics, CAS, Beijing 100029, China. Email: lgm@mail.iggcas.ac.cn
Abbreviations: Act, actinolite; Au, native gold; Bio, biotite; Bn, bornite; Cc, carbonate; Chl, chlorite; Cp, chalcopyrite; Gp, gypsum; Hem, hematite; Kfs, K-feldspar; Mo, molybdenite; Mt, magnetite; Py, pyrite; Q, quartz; Rut, rutile.

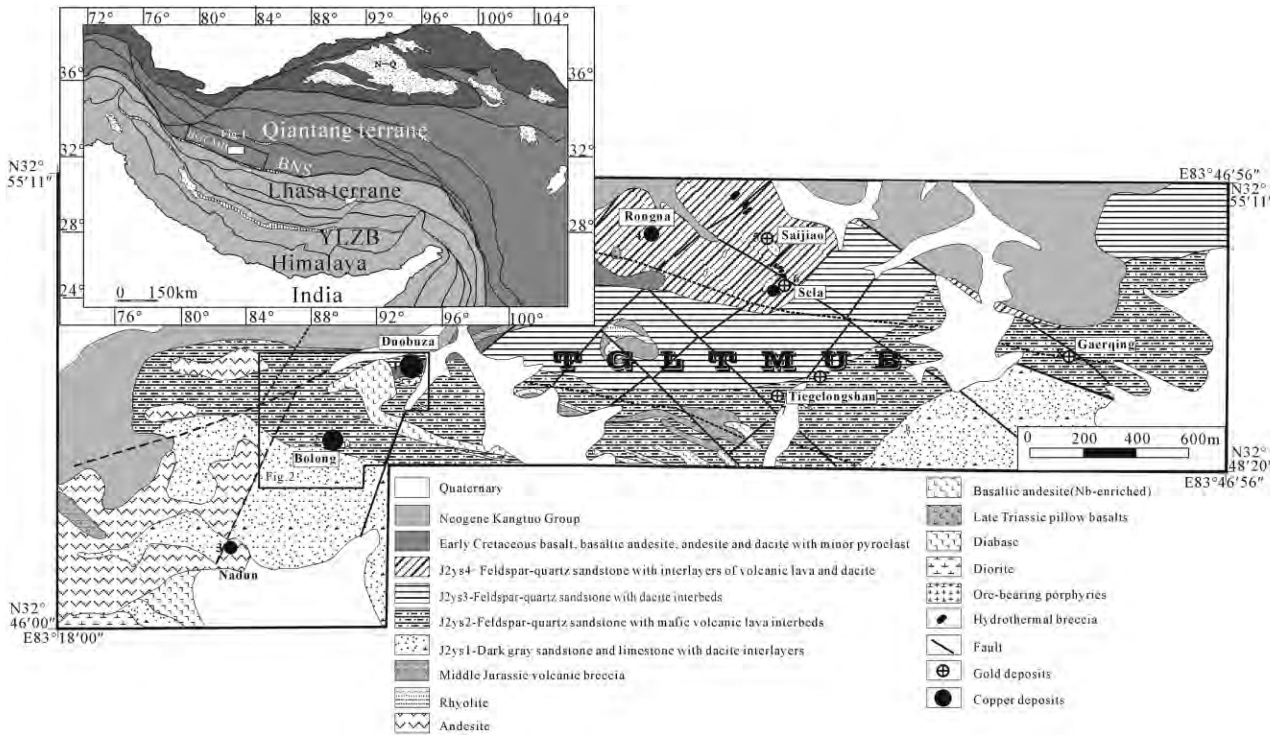


**Fig. 1** Generalized regional geologic map of the Duobuza gold-rich porphyry copper district in the Bangonghu tectonic belt. Modified from No.5 Geological Team, Tibet Bureau of Geology and Exploration (TBGE), 2003.

ore occurrence have been discovered in the ore district. They are Duobuza (about 2.7 Mt Cu at an average grade of 0.94% and 13t Au at an average grade of 0.21 g/t), Bolong (about 2.08 Mt Cu at an average grade of 0.52% and 99 t Au at an average grade of 0.41 g/t) and 135 Line. The discovery of the Duobuza district upgraded the BGCMB (Fig. 1) to the third porphyry copper belt in Tibet, following Yulong and Gangdese (Li *et al*., 2006; Qin *et al*., 2006), but the evaluation of metal potential and research of this metallogenic belt have just begun. Previous studies showed that the Duobuza deposit formed during the Late Cretaceous Neo-Tethys subduction stage (Li *et al*., 2008). Their mineralization characters and age are distinctly different from those of many porphyry Cu-Mo deposits in the Yulong and Gangdese porphyry (Hou *et al*., 2003; Rui *et al*., 2003; Qin *et al*., 2005), which are related to adakite derived from melting of lower crust during the post-collisional setting.

This paper documents, based on detailed field investigation and laboratory study, geological characteristics, intrusive rocks, hydrothermal alteration and vein systems. Then, preliminary mass balance calculation is used to estimate the bulk gains and losses of elements associated with the main alteration assemblages.

## 2. Geology

### 2.1 Regional geology setting

The Bangongco metallogenic belt is hosted by the Bangongco-Nujiang suture zone (BNS, Fig. 1), which is a 30–90 km wide and 2000 km long zone extending from Myanmar Mogok to Bangongco. The belt is the second giant ultra-basic rock belt after Tibet's Yarlung Zangbo suture zone (Shi, 2007).

According to the regional tectonic and sedimentary facies analysis, the Bangongco-Nujiang Ocean was present in the Triassic and extended into a deep oceanic basin in the Early Jurassic. The oceanic crust was then subducted northward beneath the Qiangtang terrane by the Early Cretaceous, when the Bangongco-Nujiang suture became the locus of the arc-continental collision (Huang & Chen, 1987; Kapp *et al*., 2003). Calc-alkaline intermediate-basic volcanic rocks and I-type granite formed in the north of Bangongco-Nujiang suture zone in the Early Cretaceous, and this

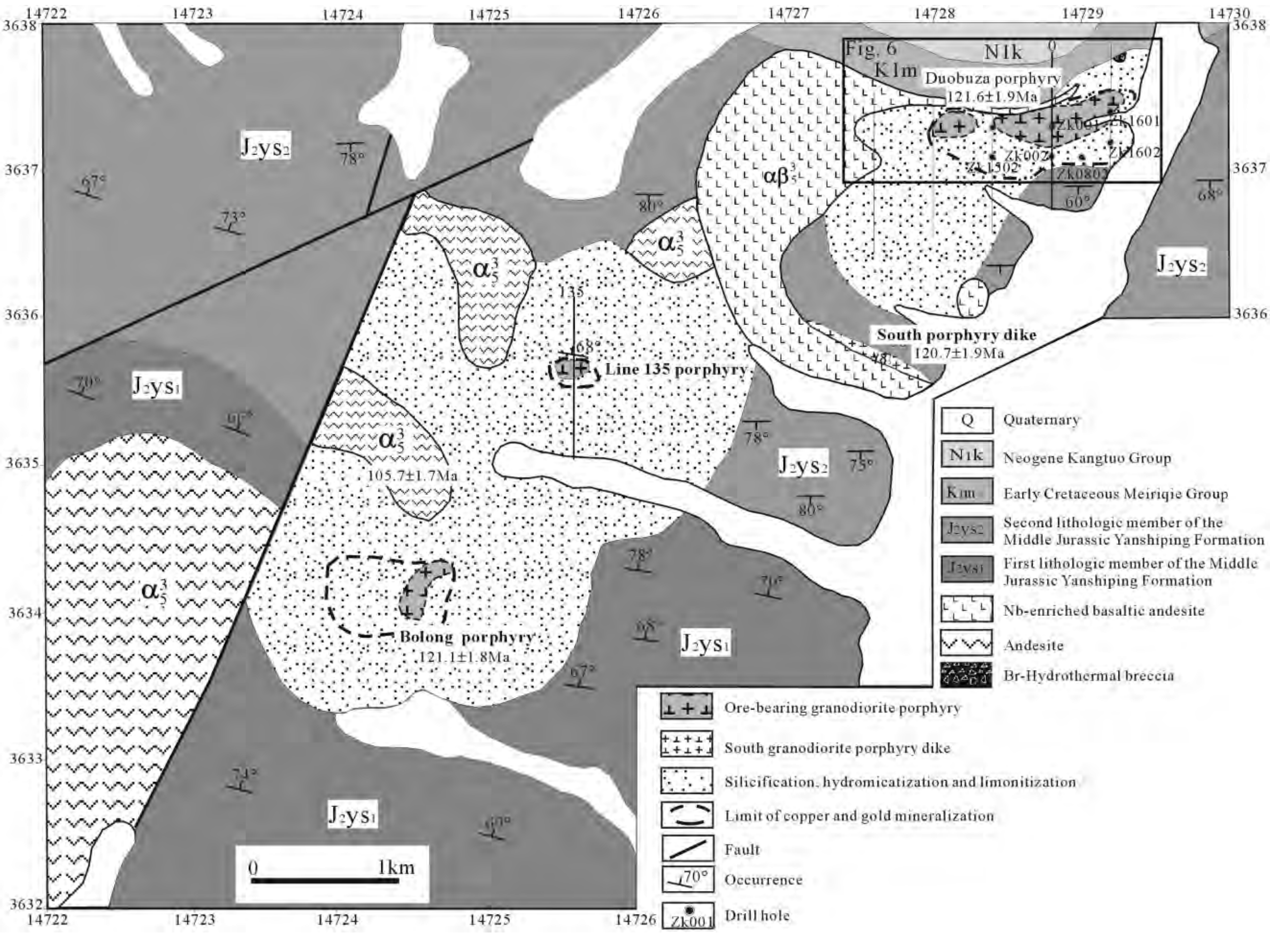


**Fig. 2** Geological map of the Duobuze gold-rich porphyry Cu district. Modified from No.5 Geological Team, Tibet Bureau of Geology and Exploration (TBGE), 2003.

magmatism is interpreted as a volcano-plutonic arc related to subduction of the Bangongco-Nujiang oceanic plate (Liao *et al*., 2005; Li *et al*., 2008). The available geochronological studies (Li *et al*., 2011b) suggest that the porphyry Cu mineralization in the Duobuza district was related to the northward subduction of this oceanic plate.

Within the Bangongco metallogenic belt, three ore-forming porphyries are equidistantly distributed in a northeasterly direction (Figs 1, 2). There are some high sulfidation epithermal Cu-Au deposits (Nadun and Tiegeshan), and Cu-Au-bearing breccia pipe deposits (Saijiao and Sela), the Gaerqin Au and placer Au deposits in the belt (Fig. 1).

## 2.2 Geology of ore district

The outcropped strata in the Duobuza district are mainly made up of the Middle Jurassic Yanshiping Formation, Early Cretaceous Meiriqie Group and the Neogene Kangtuo Group (Fig. 2). The Yanshiping Formation is composed of a volcanic and clastic littoral facies and intermediate-acidic sub-volcanic rocks. The Meiriqie Group is more than 500 m thick, and is characterized by lavas, of mostly basalt and basaltic andesite (Fig. 3a–d), interbedded with volcanic-clastic rocks. U-Pb zircon ages of intermediate-basic lavas of the Group are dated as 118.1 ± 1.6 Ma and 111.9 ± 1.9 Ma (Li *et al*., 2011b). The Kangtuo Group is composed of brown and red colored clay and sandy gravel, and is distributed in the north of the deposit, overlying unconformingly the Yanshiping Formation and Meiriqie Group.

## 2.3 Intrusive rocks

Early Cretaceous intrusions are stocks, dikes and sheets bodies of intermediate-felsic igneous rocks,

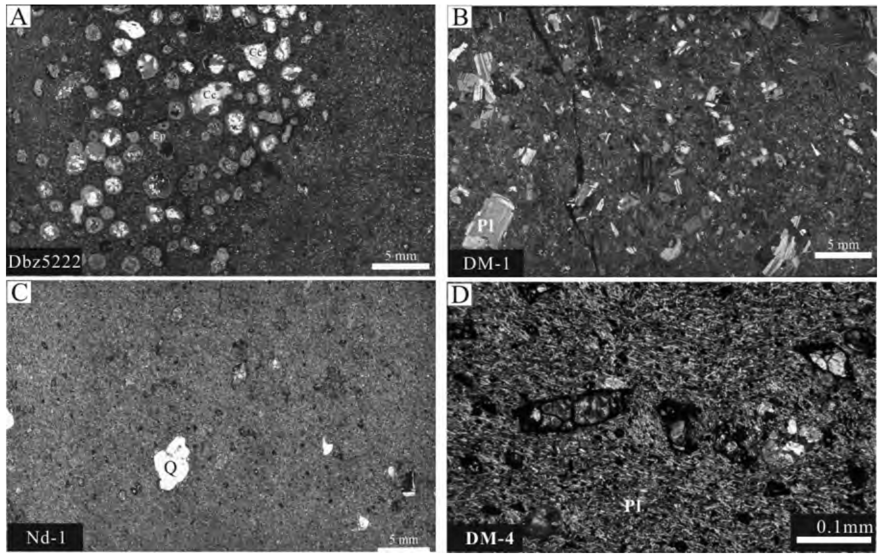


**Fig. 3** Photomicrographs of volcanic rocks in the Duobuza district. (a) Basaltic andesite located in the central part of the district, containing abundant amygdules consisting of epidote, calcite and quartz (XPL). (b) Plagioclase phenocryst-rich andesite from eastern part of the district (XPL). (c) Andesite from the northern part of the Bolong gold-rich porphyry copper deposit, containing phenocrysts of quartz, plagioclase and hornblende (XPL). (d) Basaltic andesite located in the center of the Duobuza gold-rich porphyry copper deposit. Abbreviations: Cc: calcite, Ep: epidote, Pl: plagioclase, (q) Quartz. XPL: cross-polarized light.

including diorite, quartz diorite porphyry and granodiorite porphyry that intruded in the Yanshiping Formation and Meiriqie Group. The mineralization is mainly hosted in small stock-like granodiorite porphyry (Fig. 2), quartz diorite porphyry and hydrothermal breccia. The characteristics of these rocks are listed in Table 1 and Figure 4.

The Duobuza stock (Fig. 2) mainly consists of granodiorite porphyry, which is the major ore bearing rocks in the district, with irregular fusiform outcrop 200 m × 1000 m. This porphyry shows porphyritic texture, with about 60 vol.% phenocrysts ranging from 1.6 to 4.6 mm in size including plagioclase, quartz, K-feldspar and minor hornblende and biotite. The groundmass consists of aphanitic quartz, plagioclase and biotite (Fig. 4a).

The Duobuza quartz diorite porphyry is one of the ore-bearing porphyries, which is located at the 135 prospecting line, with outcrops in 50 m by 100 m (Fig. 2). The porphyry is intensely altered, with mineral assemblage of plagioclase and quartz phenocrysts in the aphanitic groundmass of quartz, plagioclase and biotite. The plagioclase phenocrysts are altered to clay minerals (Fig. 4b).

The Bolong granodiorite porphyry is located at the southwestern part of the ore district, with an outcrop in 300 m by 200 m, which intruded in the Yanshiping Formation (Fig. 2). This porphyry contains phenocrysts ranging from 1 to 5 mm in size. For intense alteration, plagioclase is completely replaced by clay minerals, and the mafic minerals are altered to chlorite (Fig. 4c).

The granodiorite porphyry dike is located at the southern part of the ore district, with outcrops 700 m by 140 m. The length of phenocrysts ranges from 2 to 5 mm, and they include plagioclase, quartz, hornblende and biotite in the aphanitic groundmass (Fig. 4d).

Hydrothermal breccia is located at the northeast of Duobuza granodiorite porphyry, with outcrops 50 m by 50 m. The breccia is composed of angular to subrounded clasts with the size range from 1 mm to several tens of centimeters. These clasts consist mainly of intensely altered granitic rocks, while the matrix is mainly hydrothermal minerals with abundant iron oxide and clay minerals.

The geochemical data from Li *et al*. (2008) and Xin *et al*. (2009) show that ore-bearing porphyries have dacitic composition with adakitic affinity. All the published geochronology data (She *et al*., 2009; Li *et al*., 2011b) are summarized in Figure 5: zircon U-Pb ages of the ore-bearing and barren granodiorite porphyries range from 120.7 ± 1.9 to 121.6 ± 1.9 Ma; $^{40}Ar$-$^{39}Ar$ ages of hydrothermal biotite, K-feldspar and sericite range

**Table 1** Petrographic characteristic of intrusions in the Duobuza district

| Intrusion | Duobuza ore-bearing porphyry stock | Line 135 ore-bearing porphyry stock | Bolong ore-bearing porphyry stock | South Barren porphyry dike | Hydrothermal breccias body |
|---|---|---|---|---|---|
| Location | Eastern section of the district | Center of the district line 135 | West-southern section of the district | 1.5 km south from Duobuza | 100 m northeast of the Duobuza stock |
| Exposed size at surface | 0.2 km × 1 km | 0.05 km × 0.1 km | 0.3 km × 0.2 km | 0.14 km × 0.8 km | 0.05 km × 0.05 km |
| Sample | DBZJ2-1 | DBZ135-1 | Dw-2–8 | 06DBZ-20 | DbzT6-3J |
| Rock types | Granodiorite porphyry | Quartz diorite porphyry | Granodiorite porphyry | Granodiorite porphyry | Hydrothermal breccia |
| Structure or texture | Porphyritic | Porphyritic | Porphyritic | Porphyritic | Brecciated |
| Compositions of phenocryst and size | Pl: 1.6–4.6 mm, 30%<br>Kfs: 1.65–2.3 mm, 10%<br>Q: 2.7–3.6 mm, 10%<br>Hbl: 1.4–2.8 mm, 5%<br>Bt: 1–2.2 mm, 5% | Pl:1.3–5 mm, 30%<br>Q:1–3 mm, 5%<br>Bt:1.2 mm, 3% | Pl:2–4 mm, 30%<br>Q:1–5 mm, 10% | Pl:1–3 mm, 30%<br>Q:1–5 mm, 10%<br>Hbl: 2–4 mm, 10%<br>Bt: 1–2 mm, 5% | Fragments consisted of angular and subrounded altered rocks ranging from 1 mm to tens of centimeters |
| Groundmass | Q + Pl + Bt, 0.01–0.09 mm | Q + Pl + Bt, 0.01–0.05 mm | Q + Pl + Kfs, 0.01–0.1 mm | Q + Pl + Kfs + Bt, 0.01–0.05 mm | Cement: consisting of Fe-oxide, aphanitic minerals and clay |
| Alteration at surface | Silicification and argillic alteration | Argillic alteration | Silicification and argillic alteration | Fresh | Silicification and limonitization |
| Mineralization | Cu-Au | Cu-Au | Cu-Au | barren | Au |
| Age† | 121.6 ± 1.9 Ma | inferred 121 Ma | 121.1 ± 1.8 Ma | 120.7 ± 1.9 Ma | |

†Age data from Li *et al.*, (2011b).

from 115.2 ± 1.1 to 119.2 ± 1.1 Ma; Re-Os age of molybdenite yields 118.0 ± 1.5 Ma, indicating an early Cretaceous metallogenic event. These data show that the Duobuza and Bolong granodiorite porphyry stocks emplaced contemporaneously. The volcanic rocks with ages ranging from 106.4 ± 1.4 to 118.1 ± 1.6 Ma are younger than the porphyry ages.

## 3. Methods

Samples used for the study of petrography, alteration and mineralization and hydrothermal veins were collected from drillholes and outcrops from the Duobuza deposit (Fig. 6). A total of 72 polished thin sections and 84 polished sections were prepared. To investigate the geochemistry of altered and fresh rocks, eight representative samples were collected from drillhole cores. Major elements were determined on a Shimadzu XRF-1500 X-ray fluorescence spectrometer using fused glass disks, with precision better than 5%. Trace element composition is analyzed by ICP-MS (Finnigan ELEMENT-2) after acid digestion of samples in a Teflon bomb. The analyses were performed at the State Key Laboratory of Lithospheric Evolution and Key Laboratory of Mineral Resources, both in the Institute of Geology and Geophysics, Chinese Academy of Sciences. The analysis of minor element contents below-mentioned was performed at the National Research Center of Geoanalysis, Beijing. Sulfur content was determined using high-frequency infrared absorption spectrometry; Au content was analyzed by ICP-MS (Excell); The contents of As, Sb, Se and Hg were determined by atomic fluorescence spectrometry (AFS-830a and XGY-1011); Sn and Ag are analyzed by ICP-AES (atomic emission spectrometry). The analytical results are shown in Table 2.

## 4. Duobuza gold-rich porphyry copper deposit

### 4.1 Orebody

Two main gold-rich porphyry deposits are located at the Duobuza district, Duobuza and Bolong. They share the similar features of ore-bearing porphyries, hypogene alteration and mineralization. Characteristics of the hypogene alteration, hydrothermal system and mineralization of the Duobuza deposit are studied.

Extensive hydrothermal mineralization occurs at the Duobuza granodiorite porphyry and the Yanshiping Formation along the intrusive contact. At present, the

 

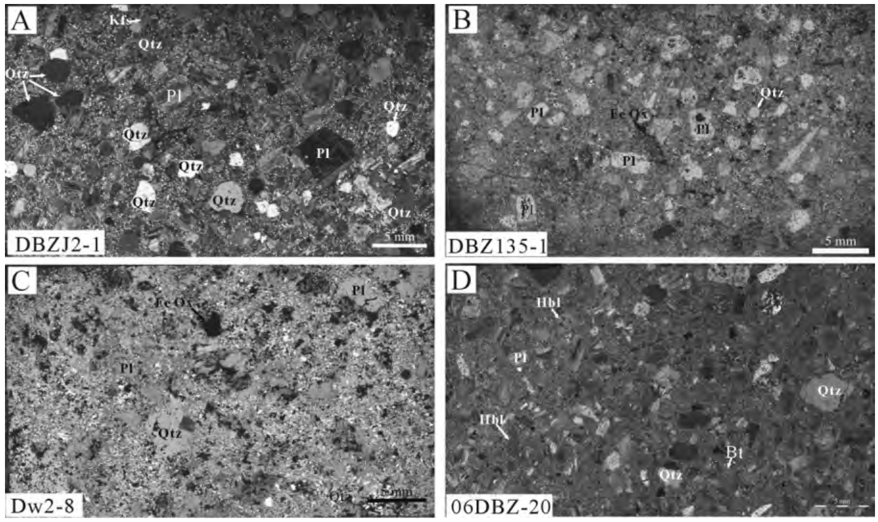


**Fig. 4** Photomicrographs of the main intrusions at the Duobuza deposit. (a) Duobuza ore-bearing granodiorite porphyry with abundant plagioclase and quartz phenocrysts (XPL). (b) Intensely altered quartz diorite porphyry, located in the center line 135 of the district, with clay minerals replacing plagioclase (XPL). (c) Bolong ore-bearing granodiorite porphyry, showing complete destructive alteration of plagioclase and silicification (XPL). (d) South Barren granodiorite porphyry dike, having phenocrysts of plagioclase, quartz and hornblende (XPL). Abbreviations: Bt: biotite, Fe-O: iron oxide, Hbl: hornblende, Kfs: K-feldspar. XPL: cross-polarized light. See others in Figure 3.

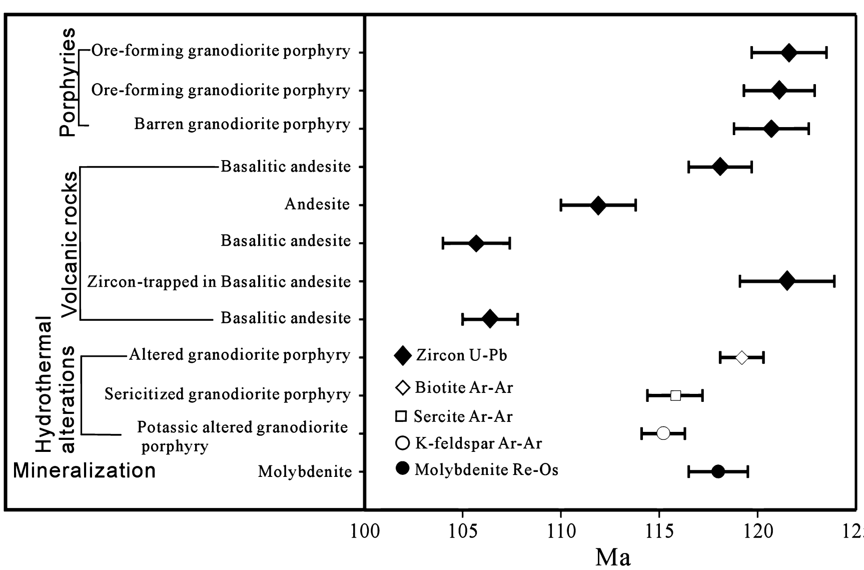


**Fig. 5** Ages of the Early Cretaceous volcanic and plutonic host rocks of the Duobuza deposit. Sources of data are Li *et al*. (2011b) except Re-Os age of molybdenite from She *et al*. (2009).

confirmed orebodies are about 100~400 m × 1400 m (Fig. 6), with a vertical extent of 500 m. The orebody strikes approximately east–west and dips northward with dip angles ranging from 65° to 80°. Spatially, the Cu and Au mineralization is closely related in the ore-bearing porphyry (Fig. 7). A 60–70 m thick supergene enrichment zone with grades of 1.17% Cu, 0.28 g/t Au, which mainly consists of malachite, azurite, copper oxides, limonite, and chalcocite, is present in the Duobuza district.

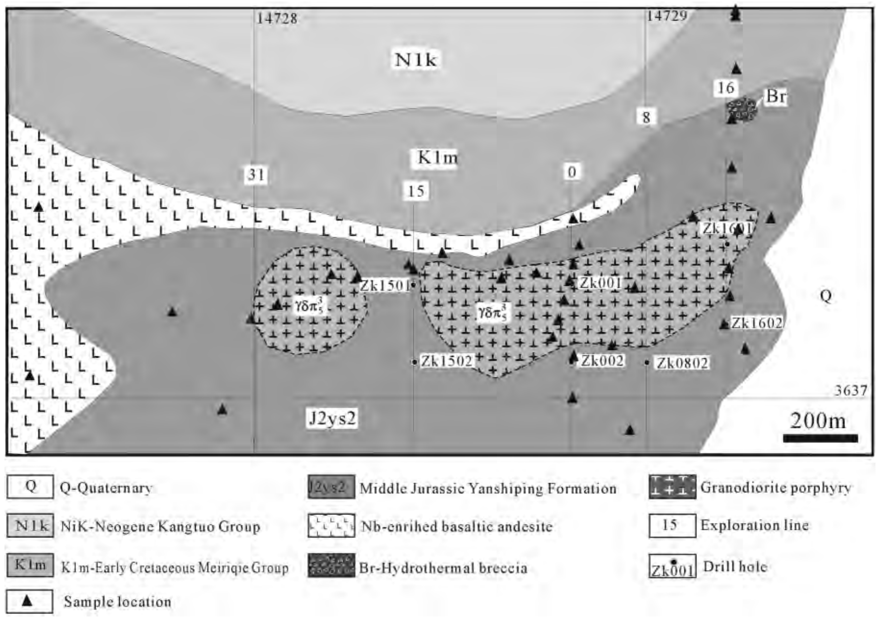


**Fig. 6** Geologic map of the Duobuza gold-rich porphyry copper deposit. Modified from No.5 Geological Team, Tibet Bureau of Geology and Exploration (TBGE), 2003.

## 4.2 Alteration types

The ore-forming porphyry stocks and the wall rocks, include sodic alteration, potassic alteration, silicification, chloritization, sericitization and argillization (Fig. 8). Main characteristics of the alteration in the deposit are summarized in Table 3.

Sodic alteration is primarily found in the form of crack-filling and reacted rim of plagioclase phenocrysts (Fig. 9a, b). Albite replacing the plagioclase phenocrysts is relatively lower in the composition proportion of $Na_2O$, and higher in $SiO_2$, $Al_2O_3$ and FeO than those substituting plagioclase matrix, both having Ab ranging from 91.5 to 99.7 (Li *et al*., 2012).

Potassic alteration is characterized by dispersed K-feldspathization, rather than secondary biotite in the deposit. This alteration zone is mainly located in the central and deep section of the porphyry stocks, superimposed by chloritization in the later hydrothermal stage (Fig. 8). This alteration zone contains biotite veins, quartz + chalcopyrite + magnetite veins. The hydrothermal magnetite is extraordinarily developed with chalcopyrite in the potassic alteration. Petrographic studies suggest chalcopyrite formed at the same time as or later than magnetite.

Sparsely disseminated secondary biotite replaced hornblende, magmatic biotite, and other Mg-Fe silicates (Fig. 9c, d). Hydrothermal biotite occurs as quartz + biotite + chalcopyrite and biotite veinlets (Fig. 9e). Electron microprobe analysis demonstrates that the composition of disseminated and vein-type biotite are identical with high $X_{Mg}$ [Mg/(Mg + Fe)] values (Li *et al*., 2012).

Replacement of phenocrysts (Fig. 9f, mainly plagioclase) and matrix (Fig. 9g) is the principal occurrence of the secondary K-feldspar. Reacted-rim of some phenocrysts of plagioclase is observed (Fig. 9f). K-feldspar-only veinlets and quartz + K-feldspar veinlets are another mode of occurrence of K-feldspar (Fig. 9h, i). In addition, K-feldspar envelopes are visible along some of the quartz-magnetite veins. Most K-feldspars show high Or (75.1–96.9%), and low Ab (3.0–24.4%) and An (0–0.6%) (Li *et al*., 2012).

On the distal part of the Duobuza porphyry system, propylitic alteration is developed in the mafic-intermediate lavas and tuff (Fig. 8). The vesicles of basaltic volcanic rocks are filled with carbonate, quartz, epidote and other minerals with amygdaloidal structure. The Fe-Mg minerals are altered to chlorite and epidote, accompanied by pyrite and minor chalcopyrite.

Chlorite, a widely distributed alteration mineral in the ore district, often occurs with pervasive silicification and sometimes with phyllic alteration. Silicification-chloritization alteration is located in the middle section of orebodies overlying the potassic

 

**Table 2** Whole-rock geochemical data of least and various hydrothermally altered rocks

| Sample | Least altered | Potassic alteration (biotite and K-feldspar) | | Silicification-chloritization alteration | | | Argillic alteration (kaolinite-illite) | |
|---|---|---|---|---|---|---|---|---|
| | Zk002-437 | ZK002-371 | Zk002-414 | Zk002-270 | Zk002-221 | ZK001-164 | ZK001-80 | DbzJ2-2 |
| $SiO_2$ (%) | 67.2 | 76.27 | 63.28 | 69.02 | 69.21 | 72.61 | 65.08 | 65.82 |
| $TiO_2$ | 0.34 | 0.16 | 0.09 | 0.24 | 0.25 | 0.2 | 0.31 | 0.33 |
| $Al_2O_3$ | 14.87 | 9.69 | 17.45 | 14.27 | 14.57 | 10.06 | 13.79 | 16.07 |
| $Fe_2O_3$ | 0.76 | 0.69 | 0.18 | 0.59 | 0.31 | 2.62 | 2.84 | 3.06 |
| FeO | 1.65 | 0.8 | 0.47 | 1.16 | 1.07 | 1.98 | 2.51 | 2.12 |
| MnO | 0.1 | 0.17 | 0.14 | 0.36 | 0.07 | 0.04 | 0.06 | 0.03 |
| MgO | 1.48 | 0.65 | 0.38 | 1.12 | 1.08 | 0.88 | 1.57 | 1.38 |
| CaO | 2.59 | 2.82 | 2.99 | 2.64 | 2.25 | 1.75 | 2.55 | 2.13 |
| $Na_2O$ | 1.75 | 0.26 | 1.05 | 0.27 | 1.88 | 1.29 | 1.58 | 2.93 |
| $K_2O$ | 4.89 | 4.92 | 10.11 | 5.78 | 6.09 | 4.61 | 5.43 | 3.46 |
| $P_2O_5$ | 0.11 | 0.04 | 0.03 | 0.09 | 0.08 | 0.08 | 0.09 | 0.13 |
| LOI | 3.62 | 2.85 | 3.18 | 3.79 | 2.5 | 3.13 | 3.35 | 1.82 |
| TOTAL | 99.35 | 99.32 | 99.35 | 99.32 | 99.36 | 99.25 | 99.17 | 99.29 |
| S (%) | 0.6 | 0.94 | 0.9 | 0.57 | 0.58 | 1.4 | 1.13 | 0.032 |
| Co (ppm) | 5.56 | 1.7 | 1.67 | 2.99 | 2.77 | 4.02 | 5.16 | 5.75 |
| Ni | 8.15 | 6.45 | 4.03 | 7.77 | 7.31 | 6.34 | 6.59 | 9.23 |
| Cu | 892 | 5289 | 2356 | 1614 | 1637 | 6056 | 6595 | 1937 |
| Zn | 37.9 | 32.5 | 53.3 | 144 | 20.1 | 38.8 | 32.8 | 101 |
| Mo | 32.9 | 55.3 | 47.0 | 23.9 | 11 | 0.95 | 3.04 | 5.96 |
| W | 2.27 | 2.96 | 2.68 | 4.78 | 2.95 | 2.8 | 1.24 | 1.71 |
| Tl | 1.07 | 1.54 | 1.98 | 1.83 | 0.98 | 0.67 | 0.93 | 0.5 |
| Pb | 7.55 | 28.4 | 62.3 | 49.9 | 8.23 | 8.8 | 10.2 | 16 |
| As | 0.5 | 0.25 | 0.34 | 1.32 | 0.23 | 3.41 | 0.32 | 0.3 |
| Sb | 0.07 | 0.12 | 0.13 | 0.14 | 0.09 | 0.27 | 0.24 | 0.18 |
| Hg | 0.01 | 0.02 | 0.02 | 0.01 | 0.02 | 0.02 | 0.01 | 0.02 |
| Se | 0.35 | 0.49 | 0.38 | 0.47 | 0.43 | 2.79 | 0.45 | 0.26 |
| Sn | 0.72 | 2.08 | 0.57 | 1.42 | 0.63 | 1.70 | 1.19 | 0.64 |
| Ag | 0.18 | 1.1 | 0.52 | 1.77 | 0.49 | 0.59 | 1.46 | 0.28 |
| Au | 0.02 | 0.1 | 0.06 | 0.06 | 0.05 | 0.32 | 0.35 | 0.11 |
| Sc | 8.09 | 4.7 | 1.89 | 5.38 | 6.32 | 4.91 | 8.19 | 6.89 |
| V | 61.84 | 32.9 | 24.1 | 49.84 | 47.55 | 65.48 | 83.18 | 75.68 |
| Cr | 5.43 | 3.94 | 4.55 | 4.22 | 5.25 | 3.67 | 4.51 | 5.06 |
| Ga | 14.18 | 8.22 | 12.78 | 12.72 | 12.62 | 11.51 | 15.22 | 17.57 |
| Rb | 180.77 | 188.33 | 334.08 | 226.16 | 178.64 | 123.16 | 157.66 | 96.33 |
| Sr | 260.41 | 121.2 | 276.71 | 131.55 | 322.24 | 201.09 | 280.11 | 429.21 |
| Y | 10.64 | 4.52 | 7.03 | 8.87 | 8.44 | 9.18 | 9.11 | 9.66 |
| Zr | 91.92 | 53.37 | 86.03 | 74.27 | 82.5 | 66.78 | 102.9 | 106.69 |
| Nb | 7.54 | 4.69 | 3.35 | 6.1 | 6.60 | 5.2 | 7.53 | 6.88 |
| Cs | 12.85 | 5.3 | 7.95 | 8.64 | 10.2 | 5.22 | 7.13 | 11.05 |
| Ba | 864.12 | 891.74 | 1553.45 | 888.95 | 866.38 | 545.1 | 547.93 | 534.28 |
| La | 14.29 | 6.72 | 21.39 | 13.55 | 17.21 | 10.92 | 12.64 | 12.71 |
| Ce | 25.33 | 10.83 | 34.23 | 23.47 | 29.72 | 20.35 | 22.31 | 22.22 |
| Pr | 2.75 | 1.15 | 3.43 | 2.52 | 3.12 | 2.30 | 2.38 | 2.38 |
| Nd | 10.34 | 4.2 | 11.16 | 8.97 | 10.77 | 8.67 | 8.75 | 8.92 |
| Sm | 1.98 | 0.79 | 1.85 | 1.65 | 1.88 | 1.73 | 1.69 | 1.84 |
| Eu | 0.7 | 0.47 | 0.78 | 0.68 | 0.69 | 0.38 | 0.51 | 0.63 |
| Gd | 1.93 | 0.77 | 1.66 | 1.6 | 1.68 | 1.69 | 1.66 | 1.95 |
| Tb | 0.3 | 0.12 | 0.23 | 0.24 | 0.25 | 0.25 | 0.25 | 0.29 |
| Dy | 1.69 | 0.63 | 1.2 | 1.33 | 1.36 | 1.35 | 1.37 | 1.63 |
| Ho | 0.35 | 0.12 | 0.22 | 0.28 | 0.27 | 0.28 | 0.28 | 0.33 |
| Er | 1.01 | 0.39 | 0.65 | 0.83 | 0.79 | 0.78 | 0.81 | 0.92 |
| Tm | 0.16 | 0.08 | 0.11 | 0.14 | 0.14 | 0.13 | 0.13 | 0.15 |
| Yb | 1.12 | 0.56 | 0.72 | 0.95 | 0.97 | 0.8 | 0.93 | 0.99 |
| Lu | 0.18 | 0.09 | 0.12 | 0.15 | 0.16 | 0.12 | 0.15 | 0.15 |
| Hf | 2.75 | 1.62 | 2.42 | 2.27 | 2.53 | 1.91 | 2.96 | 3.23 |
| Ta | 0.54 | 0.31 | 0.15 | 0.51 | 0.54 | 0.33 | 0.55 | 0.53 |
| Bi | 0.2 | 2.53 | 2.76 | 0.37 | 0.1 | 0.27 | 1.4 | 0.13 |
| Th | 6.44 | 5.09 | 3.1 | 8.06 | 8.42 | 4.72 | 6.34 | 8.18 |
| U | 0.85 | 0.41 | 0.52 | 1.14 | 1.2 | 0.44 | 0.67 | 0.64 |

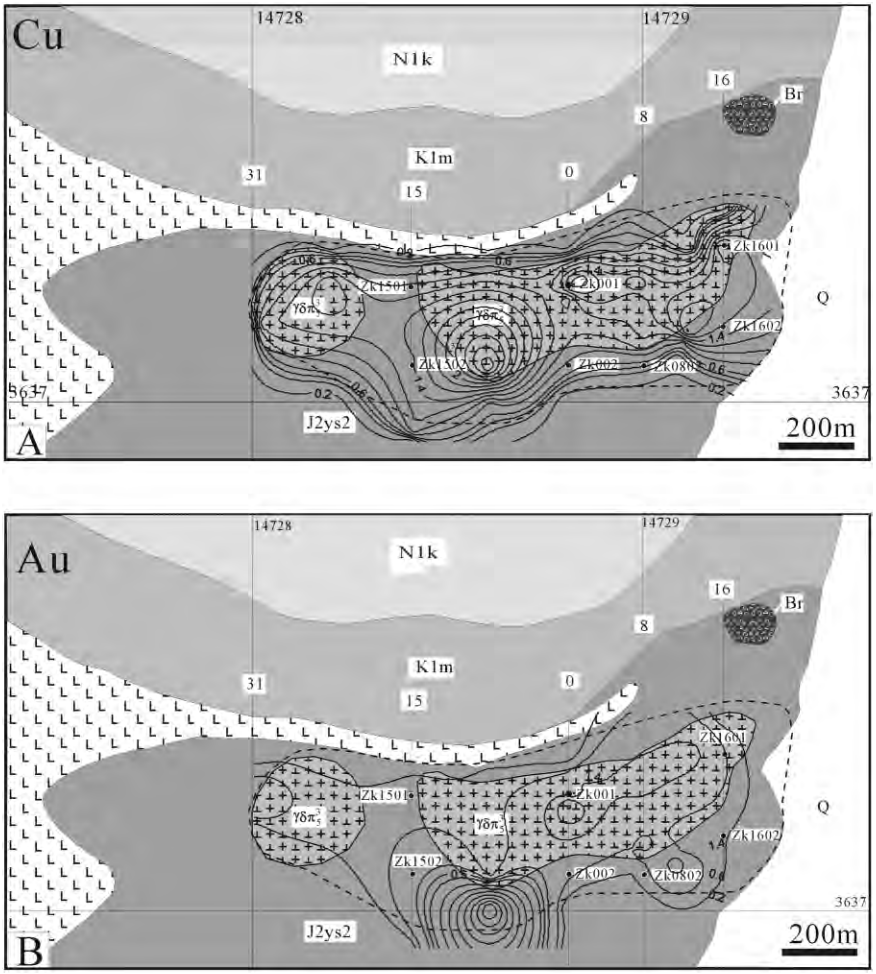


**Fig. 7** Distribution of copper (wt%) (a) and gold (ppm) (b) grades on the plane geologic map of the Duobuza deposit.

alteration zone (Fig. 8). In this alteration, ferromagnesian minerals, such as biotite, are replaced by chlorite (Fig. 9j, k), and veinlet chlorite is also well developed (Fig. 9l). Sometimes, plagioclase is altered to sericite (Fig. 9m, n). Chloritization is associated with gypsum, carbonate and chalcopyrite (Fig. 9k). EPMA studies show the chlorite of different occurrences has the same range of $X_{Mg}$ (0.55–0.70). The result indicates that most of the chlorite is identified as pycnochlorite, while the chlorite in the gypsum-carbonate-chlorite veins is ferro-penninite. The forming temperature of chlorite calculated according to the method of Cathelineau (1988) and Jowett (1991) ranges from 280°C to 340°C. However, the chlorite in the gypsum-carbonate-chlorite vein (Fig. 9k), which possibly represents the latest hydrothermal stage, formed at the range between 190°C and 220°C (Li *et al*., 2012).

Argillic alteration, overlapping the potassic zone, is shown as the breakdown of plagioclase and replacement by kaolinite, dickite and illite, which is mainly distributed in the shallow part of the deposit and its surface.

Feldspar-quartz sandstone and siltstone of the Yanshiping Formation underwent intense pervasive silicification and illite-muscovite alteration with quartz-pyrite veins (Fig. 9q).

In the hanging wall contact zone of the Duobuza porphyry, some argillaceous siltstone of the Yanshiping Formation are recrystallized to fine-grained, hornfels of biotite, quartz, chalcopyrite, pyrite and minor chlorite (Figs 8, 9r).

From the center outward of the ore-bearing porphyry, the alteration zone is horizontally divided into potassic alteration, chlorite-quartz alteration, argillic alteration,

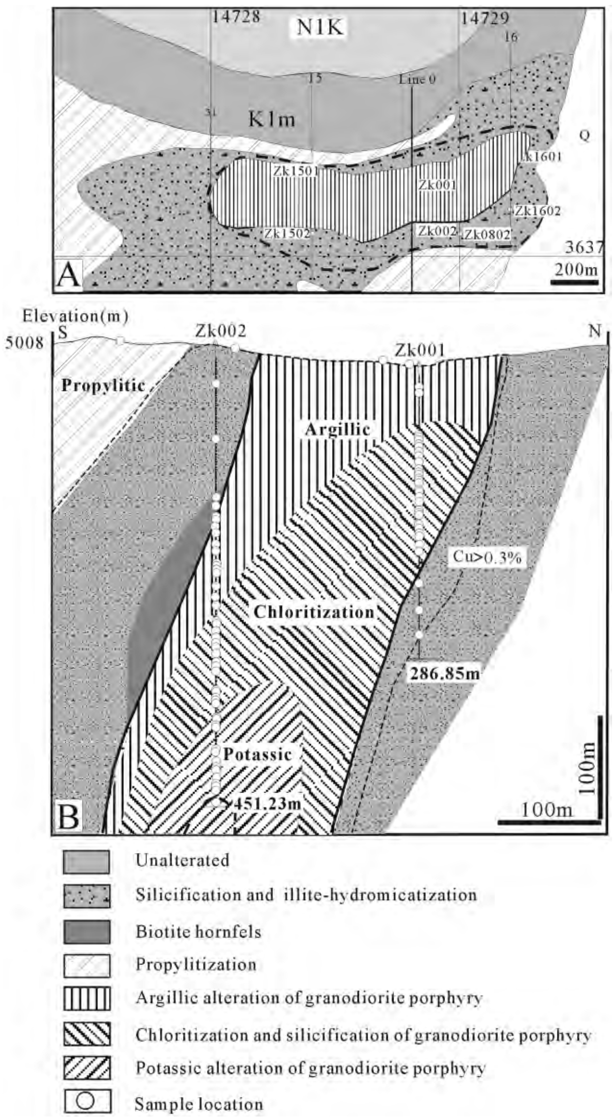


**Fig. 8** Alteration zonation of the Duobuza gold-rich porphyry copper deposit. (a) Alteration zonation at surface. (b) Alteration zonation along cross-section line 0.

illite-muscovite-hematite zones or hornfels zones, and propylitic zones. The alteration zones are vertically divided into potassic alteration, chlorite-quartz alteration and argillic alteration upwards (Fig. 8b).

## 4.3 Characteristics of hydrothermal veins and ore textures

### 4.3.1 *Characteristics of hydrothermal veins*

Alteration petrography suggests that a series of hydrothermal veins (veinlets and stockwork veins) are widely developed from the inner potassic alteration zone to the outer propylitic zone at Duobuza. Main selected characteristics are listed in Table 4.

In the potassic zone of the ore-bearing porphyry, hydrothermal veins are developed, as magnetite veinlets (Fig. 10a), biotite veins, K-feldspar-biotite-chalcopyrite-quartz veins (from wall to center are K-feldspar, biotite, quartz and chalcopyrite), magnetite-K-feldspar ± actinolite veins, quartz-magnetite-chalcopyrite veins (Fig. 10b), quartz-K-feldspar veinlets (Fig. 10c, d), K-feldspar veinlets (Fig. 10e), quartz-magnetite-biotite-K-feldspar veins (Fig. 10f), quartz-chalcopyrite veins with K-feldspar envelope (Fig. 10g) and hairline chalcopyrite veinlets (Fig. 10h). The silicification-chloritization zone includes quartz-chalcopyrite veins with oriented, continuous chalcopyrite in the center line and cutting quartz-K-feldspar veins (Fig. 10i, j), S-shape threadlike chalcopyrite stockwork veinlets and gypsum-chalcopyrite veins (Fig. 10k). Quartz-chalcopyrite-pyrite veins (Fig. 10l), quartz-pyrite veins, gypsum-chalcopyrite veins and quartz-gypsum-molybdenite-chalcopyrite veins are present in the argillic zone, and the wall rock contains quartz-magnetite veins (Fig. 10m), quartz-gypsum veins (Fig. 10n), quartz-(molybdenite)-chalcopyrite veins, quartz-pyrite veins (Fig. 10o), gypsum-chalcopyrite veins (Fig. 10p), and carbonate veins (Fig. 10n). The Duobuza deposit contains more vein types than those of other porphyry Cu deposits (Tinggong, Qulong) in the Gangdese belt (Li *et al*., 2006; Li *et al*., 2007b; Xiao *et al*., 2008). Major episodes of copper and gold mineralization are potassic alteration and chloritization stages.

### 4.3.2 *Ore textures*

The hypogene ores mainly consist of chalcopyrite, magnetite and minor pyrite; with rare chalcocite, cubanite, bornite, molybdenite, native gold and rutile. Argentite and galena occur locally. Chalcopyrite is much more abundant than pyrite and bornite. Magnetite is commonly associated with potassic alteration, and occurs as disseminated (Fig. 11a), thin veinlets (Fig. 11b) of chalcopyrite (Fig. 11c, d). Locally, chalcopyrite coexists with magnetite, and cubanite occurs as inclusions in magnetite (Fig. 11d). Both chalcopyrite and bornite commonly occur as thin veinlets (Fig. 11e–g) and dissemination (Fig. 11h). Chalcopyrite usually occurs as mineral inclusions in pyrite (Fig. 11i). Bornite is closely associated with chalcopyrite (Fig. 11i) or as inclusions in chalcopyrite. Pyrite commonly occurs as thin veins (Fig. 11h, j) or disseminated.

**Table 3** Characteristics of the main hydrothermal alteration at the Duobuza gold-rich porphyry copper deposit

| Alteration assemblage | Mineral assemblages | Main characteristics of veins | Alteration distribution |
|---|---|---|---|
| **Sodic silicate alteration**<br>Secondary albite replaces mainly plagioclase phenocryst along its rim and fissures. The albite show high contents of Ab (91.5–99.7%) with minor An (0.2–8.2%) and Or (0.1–1.1%). They also show minor amounts of FeO (0–0.36%), and negligible $TiO_2$, MnO, MgO (Li *et al*. 2010). | Albite, local calcite | No associated veins. | Locally developed |
| **Potassic silicate alteration**<br>Pervasive fine-grained hydrothermal K-feldspar and biotite affecting ore-bearing granodiorite porphyry; secondary K-feldspar replaced mainly the plagioclase phenocryst and the matrix. Moreover, secondary biotite altered mainly the primary hornblendes and biotites. Moreover, hydrothermal magnetite developed intensely in the potassic alteration zone, while chalcopyrite coexisted closely with magnetite. Pervasive fine-grained silicification shell and quartz vein-veinlets are developed. | K-feldspar, biotite, magnetite, rutile, chalcopyrite, rarely pyrite, native gold, bornite. | Quartz-chalcopyrite-magnetite veins(A-type)<br>Quartz-K-feldspar veinlets<br>Quartz-biotite-chalcopyrite veins<br>Biotite veinlets<br>Magnetite veins<br>Chalcopyrite veinlet | Potassic alteration zone developed mostly in the deep level of porphyry. |
| **Propylitic alteration**<br>Pervasive alteration including epidote-chlorite ± pyrite and rarely chalcopyrite. Carbonate, quartz, epidote and other minerals commonly fill in the vesicular basaltic andesite and gray-green basalts, basic lava of the middle Jurassic Yanshiping Formation. | Epidote, chlorite, carbonate, pyrite, rarely chalcopyrite | Quartz-magnetite (A-type)<br>Sinuous and discontinuous barren quartz veins<br>Quartz-carbonate veins<br>Gypsum veinlets | This zone occurs mainly in the basaltic andesite and andesitic volcanoclastic rocks of western and southern Duobuza. |
| **Silicification-chloritization alteration**<br>Widespread pervasive chlorite replaced mafic minerals, e.g. biotite. Within the intrusive rock, chlorite also occurs in about 1-mm cracks that cut early veins. Pervasive fine-grained silicification shell and quartz vein-veinlets also develop in the alteration assemblage. Locally plagioclase replaced by sericite and illite, | Quartz, chlorite ± sericite, illite, chalcopyrite, bornite, pyrite, native gold | Chalcopyrite veinlet<br>Quartz-chalcopyrite veins (B type)<br>Filamentous chalcopyrite veins.<br>Quartz-chlorite vein<br>Chlorite-chalcopyrite vein<br>Quartz-chlorite-chalcopyrite vein | This zone superimposes on potassic alteration zone. |
| **Argillic alteration**<br>Pervasive kaolin, dickite, illite-muscovite replacement of plagioclase, showing decomposition of feldspar. | Kaolin, dickite, illite-muscovite, quartz, chalcopyrite and rutile, locally calcite and pyrite | Quartz-chalcopyrite-molybdenite vein<br>Quartz-chalcopyrite-pyrite vein<br>Quartz-pyrite vein<br>Quartz-molybdenite vein<br>Chalcopyrite veinlet, pyrite veinlet | Argillic alteration developed at surface and within the upper level of porphyry, overprinted earlier alteration types at all scales. |
| **Silicification and illite-muscovitization**<br>Strong, pervasive silicification alteration of the feldspar-quartz sandstone and siltstones of the Middle Jurassic Yanshiping Formation, and feldspar destructive alteration of the sandstone and siltstone formed illite-muscovite. | Quartz, illite-muscovite, sericite and limonite or/and pyrite | Quartz-pyrite veins (D-type)<br>Gypsum-chalcopyrite veinlets<br>Pyrite veinlet | Widespread developed. Extends several hundreds of meters from centered porphyry. |
| **Hornfels**<br>At the porphyry upper contact, alteration observed in the sedimentary lithology involve recrystallization of muddy siltstone of the Yanshiping Formation to fine-grained, dark gray to light greenish grey hornfels containing an assemblage of biotite-quartz-chalcopyrite-pyrite with minor chlorite. | Quartz, biotite, chalcopyrite, pyrite | Pyrite veinlet<br>Chalcopyrite veinlet | Locally developed at the Duobuza porphyry upper contact. |

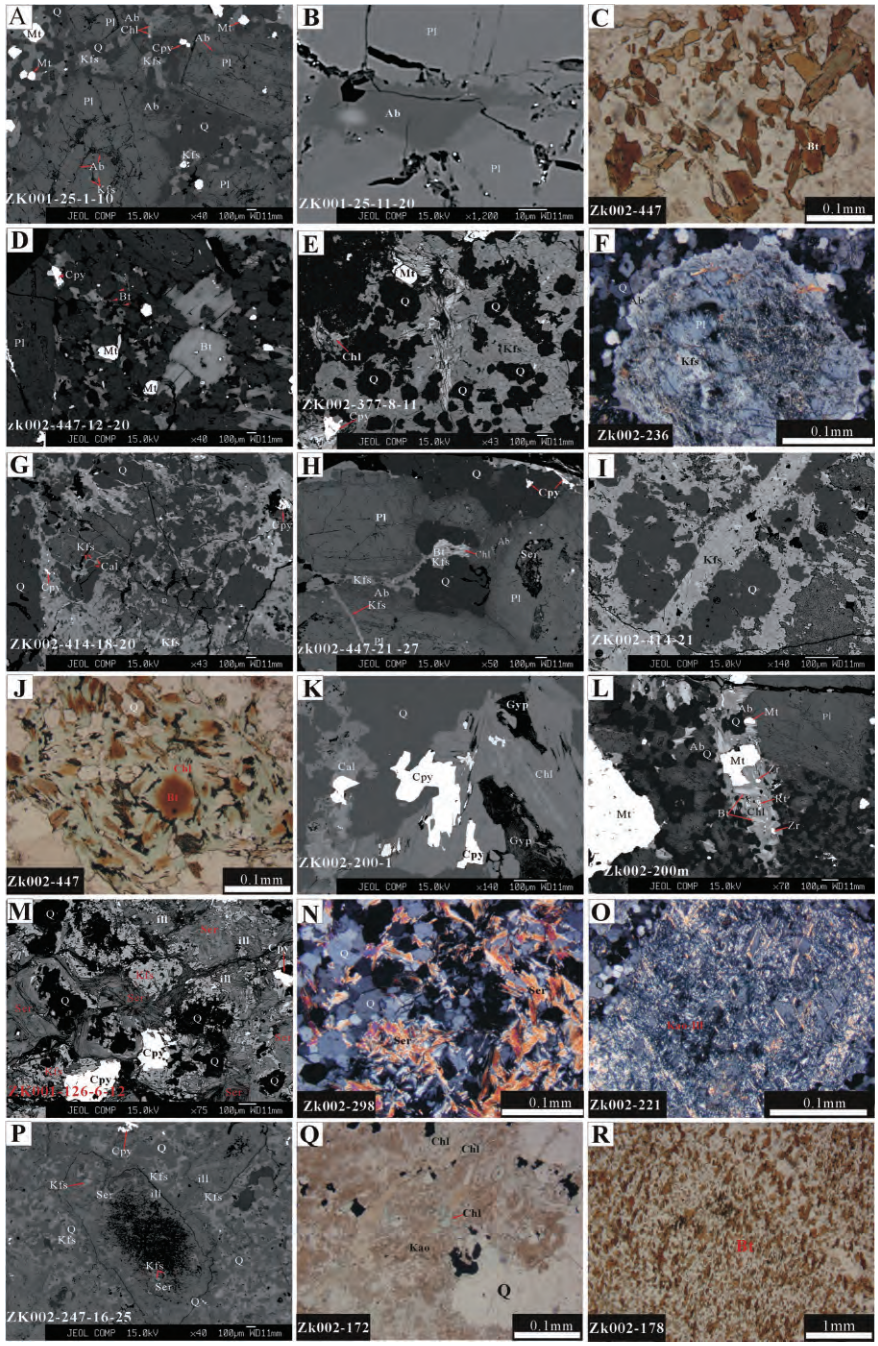

However, native gold mainly occurs as inclusions in disseminated chalcopyrite (Fig. 11k, l) and quartz (Fig. 11m) in the potassic alteration zone. Gangue minerals consist of K-feldspar, albite, quartz, sericite, chlorite, carbonate, illite and gypsum; otherwise, rare quartz-molybdenite veins are observed, and molybdenite is visible in veinlets and as disseminated texture (Fig. 11n, o). The veinlet-disseminated mineralization weakens downwards. Consequently, from ground surface downwards, the copper grade decreases.

**Fig. 9** Photomicrographs showing hydrothermal alteration at the Duobuza deposit. (a) Albite replacement along edge of plagioclase or albite veinlets filling the fissure in granodiorite porphyry, Zk001-25 m (BSE). (b) Albite replacement along intergranular plagioclase in granodiorite porphyry, Zk001-25 m (BSE). (c) Secondary biotite flake aggregates in granodiorite porphyry, Zk002-447 m (SPL). (d) Secondary biotite coexisting with magnetite and chalcopyrite near biotite phenocrysts in granodiorite porphyry, Zk002-447 m (BSE). (e) Secondary biotite veinlets in pervasive silicification and K-feldspar in granodiorite porphyry, Zk002-377 m (BSE). (f) K-feldspar replacement of plagioclase, rimmed with albite in granodiorite porphyry, Zk002-236 m (XPL). (g) Pervasive silicification and hydrothermal K-feldspar with disseminated chalcopyrite, carbonate veinlets, and plagioclase replaced by dickite in granodiorite porphyry, Zk002-414 m (BSE). (h) K-feldspar veinlets cutting plagioclase and quartz phenocrysts, and local albitization and sericitization of plagioclase in granodiorite porphyry, Zk002-447 m (BSE). (i) Pervasive silicification and secondary K-feldspar cut by K-feldspar veinlets (BSE). (j) Chlorite replacing secondary biotite in granodiorite porphyry, Zk002-447 m (SPL). (k) Chlorite replacement of biotite, with gypsum and chalcopyrite in granodiorite porphyry, Zk002-200 m (BSE). (l) Secondary biotite veinlets replaced by chlorite, coexisting with quartz, magnetite, rutile and zircon in granodiorite porphyry, Zk002-200 m (BSE). (m) Hydrothermal K-feldspar replaced by sericite and illite in granodiorite porphyry, Zk001-126 m (BSE). (n) Quartz-sericite veinlets in granodiorite porphyry, Zk002-298 m (XPL). (o) Kaolinite, illite-muscovite replacement of plagioclase phenocryst in granodiorite porphyry, Zk002-221 m (XPL). (p) Plagioclase phenocryst replaced by illite in granodiorite porphyry, Zk002-247 m (BSE). (q) Kaolinite and dickite replacement of plagioclase in a chloritized matrix in granodiorite porphyry, Zk002-172 m (SPL). (r) Pervasive chloritization in the wall rocks of basic volcanic rock, Zk002-178 m (SPL). Abbreviations: Chl, chlorite; Cpy, chalcopyrite; Kao-ill, kaolinite-illite; Mt, magnetite; Ser, sericite; Rt, rutile; Zr, zircon; BSE: backscattered electron image; SPL, single-polarized light; XPL: cross-polarized light. See others in Figures 3 and 4.

#### *4.3.3 Paragenetic sequence*

On the basis of the vein relationship and hydrothermal mineral assemblages, the hydrothermal activity is divided into five stages (Fig. 12).

**1** Potassic silicate-sulfide stage: biotitization and K-feldpathization are the most important alteration types in this stage. This stage is divided into early and late sub-stages. Biotitization is dominant in the early subs-stage, and hydrothermal magnetite (contents >15%) occurs in this sub-stage. The late sub-stage is characterized by pervasive and veinlet-type K-feldspar and Cu-Fe sulfides and gold precipitation, which is the most significant mineralization stage.

**2** Chlorite-quartz-sulfides stage (sillicfication-chloritic alteration): chlorite, silicification and local sericitization occurred in this stage. Cu-Fe sulfides precipitated as veinlets or dissemination, and native gold is occasionally visible.

**3** Argillization-sulfides stage: feldspars are replaced by dickite and kaolinite. Silicification-illite-muscovite alteration is extremely developed. The content of Cu-bearing sulfides decreases and that of pyrite increases.

**4** Quartz-carbonate-pyrite stage: gypsum and quartz-carbonate veins formed as veinlets or stockwork veins.

**5** Secondary oxidation stage: secondary enrichment zones developed in the shallow part of the deposit, which contain series of Cu-Fe oxides and clay minerals.

## 5. Alteration geochemistry and mass balance

The geochemical data of the altered and least altered rocks of the ore-bearing porphyries (Table 2) are used to quantify elemental mass transfer associated with the main alteration processes. We chose Ti, Al and Zr for mass-balance calculation since Ti, Al and Zr are regarded to be relatively immobile during hydrothermal activity (Ulrich & Heinrich, 2001; Hezarkhani, 2002; Idrus *et al*., 2009). In this work, element gains and losses on a weight basis have been calculated following Grant's approach (Grant, 1986):

$$\Delta C = (1/S) * C_i^a - C_i^f$$

$C_i^f$ and $C_i^a$ respectively represent the oxide or element content of altered and least altered rocks, S is the slope of the immobile isocon. Figure 13 is the isocon diagrams of various elements in the three alteration zone versus least altered rocks. Figure 14 shows the grains or loss of major and trace elements in the selected samples.

### 5.1 Potassic alteration zone

Comparison of the content of major and trace elements in the potassic silicate rocks (the average of

 

**Table 4** Vein Types at the Duobuza gold-rich porphyry copper deposit (listed in order of decreasing relative age)

| Vein types | Distribution | Structure | Alteration halo | Width (mm) | Gangue minerals | Ore minerals | Associated alteration zone |
|---|---|---|---|---|---|---|---|
| Magnetite vein | Widely developed in the porphyry and Locally developed in the wall rock at the porphyry upper contact. | Irregular | None | 0.1–3 | | Mt, minor Cp | Sodic, magnetite |
| Magnetite-K-feldspar ± actinolite veinlets | | Irregular | Biotite | 2–3 | Kfs, Act | Mt, Cp | |
| Quartz-magnetite-chalcopyrite veinlet | Mainly distributed in the porphyry and hanging wall silicified and chloritized alteration zone | Irregular | None | 5–10 | Q | Mt, Cp, Au | Potassic |
| Quartz-magnetite ± biotite ± K-feldspar ± chalcopyrite vein | | Irregular | None | 0.5–5 | Q, Bio, Kfs | Mt, Cp, Rut | |
| Quartz-magnetite vein | | Irregular | None | 5–10 | Q | Mt, Cp | |
| Biotite veinlet | Mainly distributed within the porphyry, and concentrated in the hanging wall silicified and chloritized alteration zone. | Irregular | None | 1 | Bio | Rut, Mt, Cp | Potassic |
| K-feldspar vein | | Irregular | K-feldspar | 3–5 | Kfs | | |
| Biotite ± K-feldspar ± quartz ± chalcopyrite vein | | Irregular | None | 2 | Bio, Kfs, Q | Cp, Rut, Hem | |
| Quartz-K-feldspar ± chalcopyrite ± bornite vein | | Irregular | K-feldspar | 1–25 | Q, Kfs, | Cp, Bn, Au | |
| Quartz-chalcopyrite vein | Mainly developed in the porphyry, rarely in the wall rock. | Continuous straight and symmetrical walls | None | 0.5–30 | Q | Cp, Au | Potassic and intermediate Argillic (chlorite-quartz) |
| Quartz-molybdenite vein | | Continuous straight | None | 1–10 | Q | Mo | |
| Quartz-chlorite vein | Mainly distributed in the porphyry and hanging wall silicified and chloritized alteration zone. | Irregular to planar | None | 2–5 | Q, Chl | Py | Chlorite-quartz and argillic |
| Chlorite-chalcopyrite vein | | Irregular to planar | None | 2–5 | Chl | Py | Argillic and chlorite-quartz |
| Quartz-chlorite-chalcopyrite vein | | Irregular to planar | None | 2–5 | Q, Chl | Cp | |
| Quartz-chalcopyrite-molybdenite vein | Widely developed in the porphyry and wall rock. | Planar | None | 2–10 | Q | Cp, Mo | Argillic and chlorite-quartz |
| Quartz-chalcopyrite-pyrite vein | | Planar | None | 2–10 | Q | Cp, Py | |
| Quartz-sericite vein | Mainly distributed in the wall rock, rarely in the porphyry. | Irregular | None | 2 | Q, Ser | Py | Argillic and silicification and illite-muscovitization |
| Quartz-pyrite vein | | Planar | None | 5–10 | Q | Py, Au | |
| Other type vein | Developed in the porphyry and wall rock. | | | | | | Developed in the all alteration zones |
| Chalcopyrite veinlet | | Planar stringer | None | 0.1–2 | | Cp | |
| Pyrite veinlet | | Planar stringer | None | 0.5 | | Py | |
| Molybdenite veinlet | | Planar stringer | None | 3 | | Mo | |
| Gypsum vein | | Not straight | None | 0.1–2 | Gp | | |
| Gypsum-quartz ± molybdenite ± bornite ± chalcopyrite | | Not straight | None | 1–3 | Gp, Q | Mo, Bn, Cp | |
| Gypsum-chalcopyrite ± pyrite vein | | Not straight | None | 5–6 | Gp | Cp, Py | |
| Carbonate vein | Mainly distributed in the wall rock. | | | | | | Propylitic |
| Carbonate ± quartz ± pyrite vein | | Irregular | None | 20 | Cc, Q | Py | |

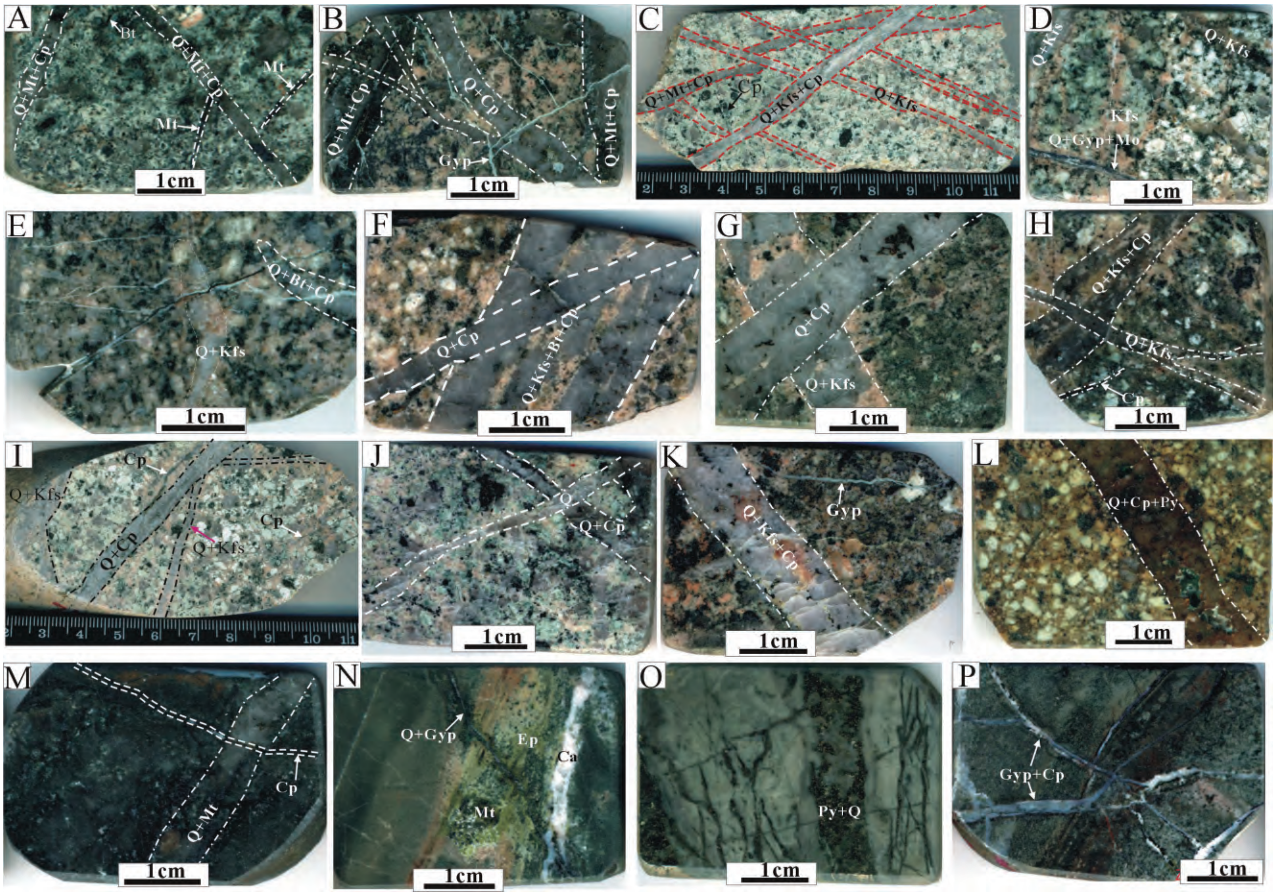


**Fig. 10** Photographs of vein types and relationships at the Duobuza deposit. Veins associated with potassic alteration. (a) Magnetite veins cut by quartz-magnetite-chalcopyrite veins. (b) Quartz-magnetite-chalcopyrite veins cut by quartz-chalcopyrite veins and then cut by gypsum veinlets. (c) Quartz-magnetite-chalcopyrite veins cut by quartz-K-feldspar veinlets, and then quartz-K-feldspar veinlets cut by quartz-K-feldspar-chalcopyrite veinlets and stringer chalcopyrite veinlets. (d) Quartz-K-feldspar veins cut by quartz-pyrite veins. (e) Quartz-gypsum-molybdenite veins cut quartz-K-feldspar veinlets. (f) Quartz-K-feldspar veins and quartz-biotite-chalcopyrite veins cross pervasive hydrothermal K-feldspar. (g) Quartz-K-feldspar-biotite-chalcopyrite veins cut by quartz-chalcopyrite veins. (h) Quartz-K-feldspar-chalcopyrite veins cut by quartz-K-feldspar veinlet and hairline chalcopyrite veins. Veins associated with chlorite alteration. (i) Quartz-K-feldspar veinlet cut by quartz-chalcopyrite veins. (j) Quartz-pyrite veins cut by quartz veinlets with sericite-chlorite alteration halo. (k) Quartz-feldspar-chalcopyrite veins cut by gypsum veinlets. Veins associated with argillic alteration of the ore-bearing porphyry. (l) quartz-pyrite-chalcopyrite veins cross granodiorite porphyry. Veins crosscut volcano-sedimentary rocks of the Yanshiping Formation. (m) Intense magnetite alteration replacing andesitic volcanoclastic sedimentary rocks, and cut by quartz-magnetite, later cut by stringer chalcopyrite veins. (n) Quartz-carbonate veins cut gypsum veinlets in the propylitic andesitic volcanoclastic sedimentary rocks. (o) Silicified andesitic volcanoclastic sedimentary rocks cut by quartz-pyrite veins. (p) Gypsum-chalcopyrite veinlets cut across andesitic volcanoclastic sedimentary rocks. Abbreviations: Py, pyrite; Mo, molybdenite. See others in the previous figures.

Zk002-371 and Zk002-414) and the least altered rocks (Zk002-437) (Fig. 14a) shows that $SiO_2$, $K_2O$, CaO, MnO, $Fe_2O_3$, Cu, Mo, Pb, Au, Rb and Ba are enriched in the altered rocks. However, FeO, MgO, $Na_2O$, Co, Ni and V deceased in the altered rocks (Fig. 14a, b), which may reflect the breakdown of plagioclase and ferromagnesian minerals. The enrichment of Si and K are related to the quartz-K-feldspar veinlets. The increase of Rb may be related to the secondary biotite in the alteration zone. Increase of CaO is related to the high-temperature carbonates replacing plagioclase. Increase of $Fe_2O_3$ accords with the presence of hydrothermal magnetite. During the potassic alteration, the Cu and Au contents distinctly

 

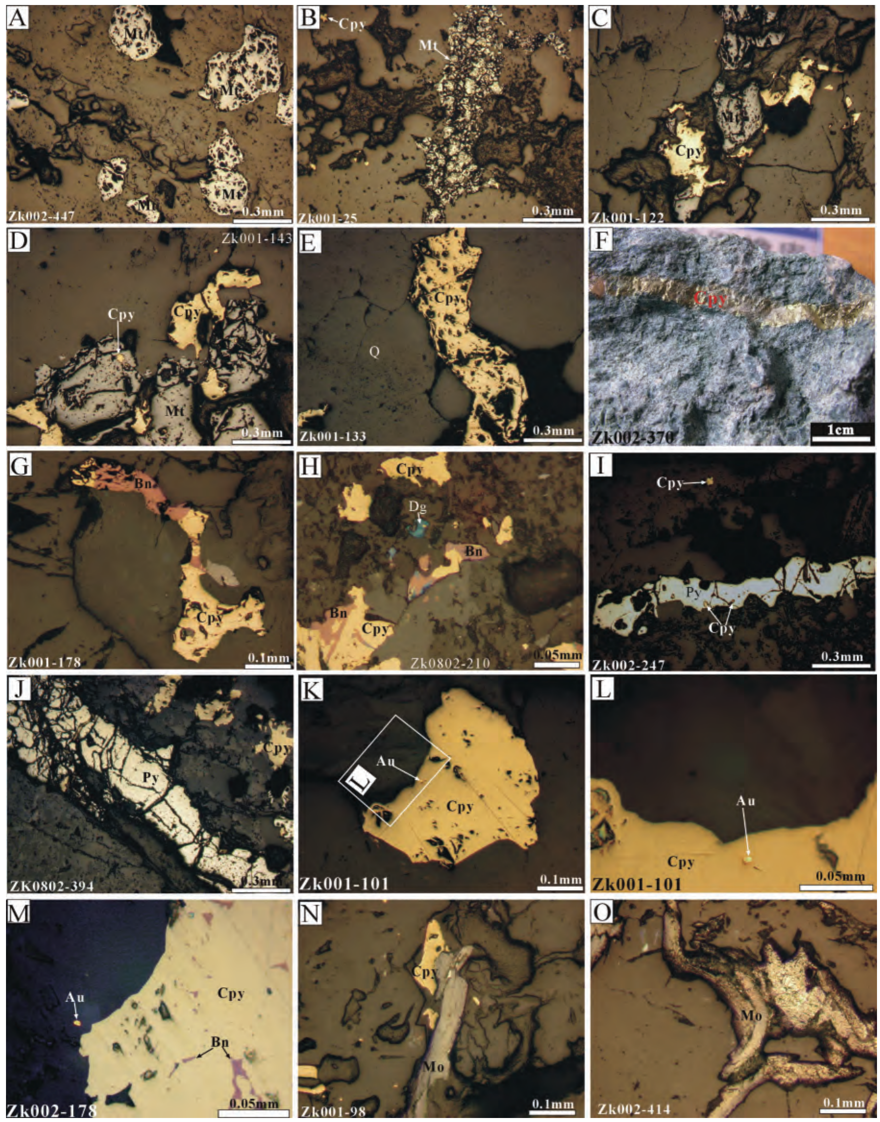


**Fig. 11** Photomicrographs of polished thin section under reflection light. (a) Disseminated magnetite in the least altered granodiorite porphyry from Zk002-447 m. (b) Magnetite veins in argillic alteration of the granodiorite porphyry from Zk001-25 m. (c) Magnetite-chalcopyrite veins cut granodiorite porphyry altered by silicification-chloritization, Zk001-122 m. (d) Magnetite coexisting with chalcopyrite and chalcopyrite inclusions in magnetite in the silicification-chloritized granodiorite porphyry, Zk001-143 m. (e) Chalcopyrite veins 0.3 mm thick in quartz-chalcopyrite veins in the silicification-chloritized granodiorite porphyry, Zk001-133 m. (f) Potassic altered granodiorite porphyry cut by chalcopyrite veinlets 0.5 mm thick, hand specimen, Zk002-370 m. (g) Silicified and chloritized granodiorite porphyry cut by chalcopyrite-bornite veinlets 0.02–0.1 mm thick, Zk001-178 m. (h) Disseminated chalcopyrite and digenite, observed intergrowth of chalcopyrite and bornite in the silicified and chloritized granodiorite porphyry, Zk0802-210 m. (i) Granodiorite porphyry cut by irregular pyrite veinlets 0.2 mm thick, chalcopyrite inclusions occurring in pyrite, associated with argillic alteration, Zk002-247 m. (j) Pyrite veinlets 0.3 mm thick, with chalcopyrite disseminated along edge of the veinlets, and pyrite filling fissures of chalcopyrite in the silicified and chloritized granodiorite porphyry, Zk0802-394 m. (k) Native gold within chalcopyrite-only grains in the silicified and chloritized granodiorite porphyry, Zk001-101 m. (l) Native gold about 5 μm in size within chalcopyrite. (m) Bornite exsolution grains in chalcopyrite. Native gold 5 μm in size adjacent to chalcopyrite in the granodiorite porphyry, associated with argillic alteration, Zk002-178 m. (n) Molybdenite-chalcopyrite veinlet 0.1 mm thick cut granodiorite porphyry, associated with argillic alteration, Zk001-98 m. (o) Potassic altered granodiorite cut by quartz-molybdenite vein. Abbreviations: Bn, bornite; Dg, digenite; Au, native gold. See others in previous figures.

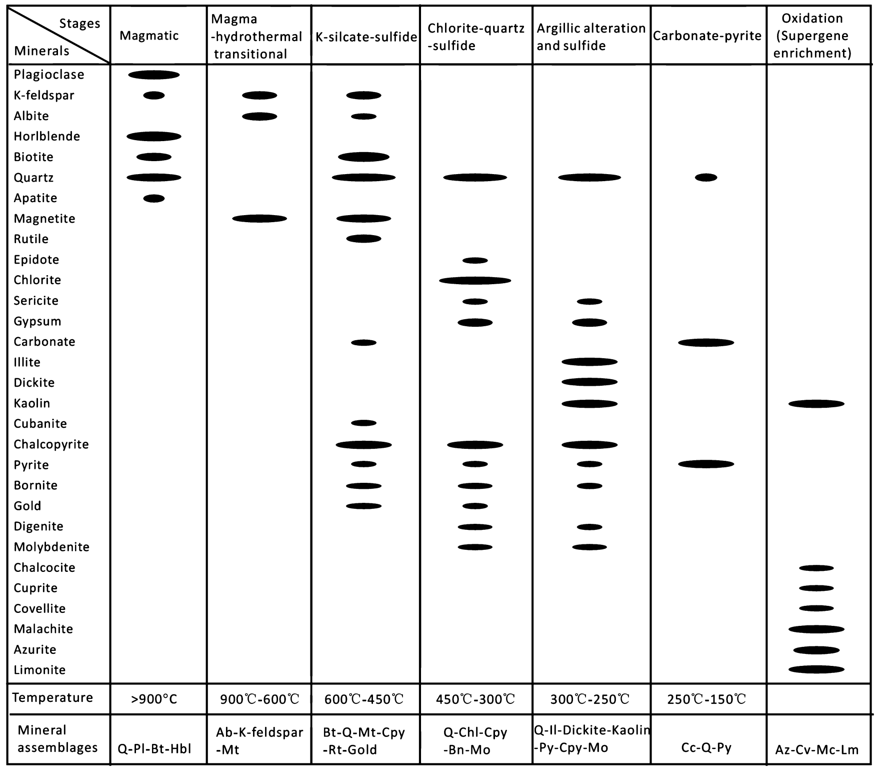


**Fig. 12** Paragenetic sequence of the Duobuza deposit (temperature intervals are based on fluid inclusion microthermometry (Li *et al*., 2007a, 2011a). Abbreviations: Az, azurite; Cv, covellite; Lm, limonite; Mc, malachite. See others in previous figures.

increase, and this is consistent with the petrographic observations.

### 5.2 Silicification-chloritization alteration

Comparison of the silicification-chloritic altered rocks (the average value of Zk002-270, Zk002-221 and Zk001-164) and the least altered rocks (Zk002-437) (Fig. 14b) shows that the contents of K, Si, Fe, Cu, Zn, Pb, Au, Rb, Sr and Ba markedly increase, while Mg and Na decrease (Fig. 14c, d). During this process, the enrichment of ore-forming elements in the altered rocks, such as Cu, Zn, Pb and Au, reflects the existence of Cu-Fe sulfides and native gold.

### 5.3 Argillic alteration

Comparison of the altered rocks (the average value of ZK001-8 and DbzJ2-2) and the least altered rocks (Zk002-437) (Fig. 14c) shows that the contents of Si, K, Ca, Mg, Rb and Ba decrease, but Fe, Na, Cu, Au and Sr increase (Fig. 14e, f). The decreased Ca content may be affected by the breakdown of plagioclase. Enrichment of Sr may be related to the abundance of gypsum occurring in the alteration process. The enrichment of Cu and Au are associated with quartz-chalcopyrite-pyrite veins.

## 6. Summary and conclusions

The ore-bearing granodiorite porphyries in the Duobuza ore district are distributed in a northeast direction, and there is about 2 km distance between them (Fig. 2). Similar occurrence, rock characteristics, alteration-mineralization styles and the same intrusion age (about 121 Ma) suggest that these ore-bearing granodiorite porphyries were derived from the same magma source.

The hydrothermal alteration, vein types and mineralization at the Duobuza gold-rich porphyry copper deposit are identical with other gold-rich porphyry copper deposits (Sillitoe, 2000). During the early stage of hydrothermal alteration and mineralization in the deposit, hydrothermal biotite, potassic feldspar, magne-

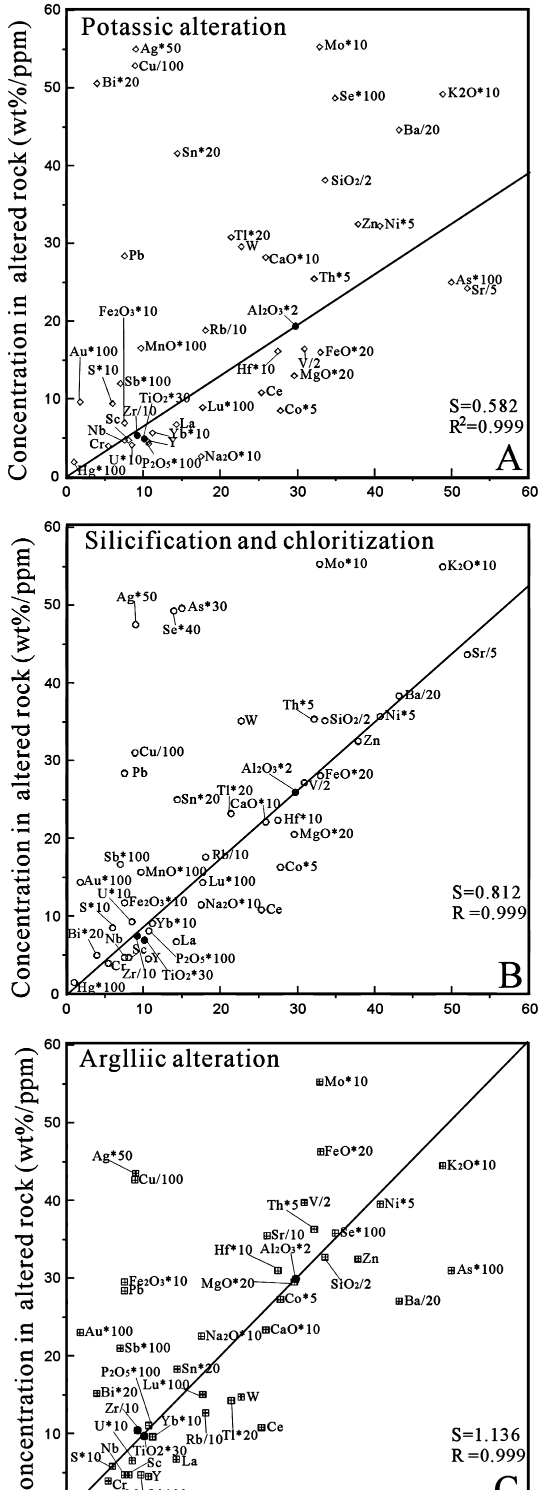


**Fig. 13** Isocon diagrams with selected and weighted elements in which the protolith (least altered Zk002-437) versus the altered samples are plotted. Various elements are multiplied or divided by a constant to fit a common scale of the diagram. Black lines (isocons) are defined by the constant ratios of immobile elements ($Al_2O_3$, $TiO_2$, Zr), which were used for the calculation of the gains and losses. Elements above these lines are enriched in the altered rock, whereas elements below the lines are depleted during alteration. Major element oxides and S in wt%, trace elements in ppm and Au in ppb.

tite and quartz coexisted with Cu-Au mineralization; copper has a positive correlation with gold; and chalcopyrite contains native gold (Fig. 10m, n). All the above phenomena demonstrate that gold and copper deposited at the same time. The dense quartz-magnetite-chalcopyrite veins (Fig. 10a, b) and quartz-K-feldspar veins occur mainly at the bottom of orebodies, which is regarded as the focused region of ascending fluid. This fluid flowing upward and outward forms the potassic alteration zone to propylitic alteration and Cu-Au mineralization. The enriched contents of copper and gold in the potassic alteration zone based on mass balance calculations (Fig. 14a, b) suggest that K-silicate alteration stage is the main mineralization stage.

The silicification-chloritization superimposed on K-silicate alteration, cut through and replaced the early stage alteration. The abundant chlorite is the main characteristic and chlorite alteration is accompanied with pervasive silicification, localized sericitization and veinlet or disseminated Cu-Fe sulfides. Chlorite always coexisted with chalcopyrite. The native gold is observed sometimes at this stage. The main effect of this mineralizing fluid is removal of Mn, Ca and Na and enrichment of Cu and Au, based on mass balance calculations (Fig. 14c, d).

Owing to the breakdown of feldspar, the formation of clay minerals, such as dickite and kaolinite, and the development of silicification-illite with dispersed silicification, are the main characteristics in the late stage of mineralization. There is still quartz-chalcopyrite veinlets accompanied with Cu sulfide decreasing in abundance and the abundance of pyrite gradually increasing. The alteration of this stage overlaps the early stage alteration and is developed well at the top of orebodies. The mass balance calculation shows that Cu and Fe were removed at this stage, which may be related to the development of quartz-chalcopyrite-pyrite veinlets at the top of orebodies.

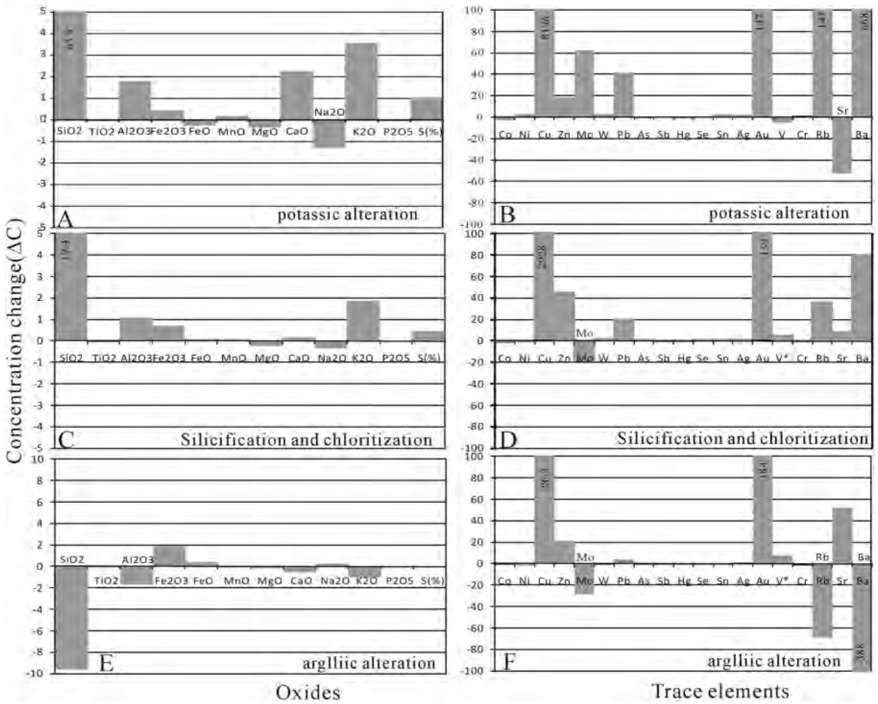


**Fig. 14** Gains and losses of major and trace elements for the main alteration assemblages.

## Acknowledgement

The research is financed by the important research direction project of the Academy of Sciences of China (KZCX2-YW-Q04-2), National Natural Sciences Foundation of China (NSFC Grants 40672068 and 40902027) and China Geological Survey project (20089932). We wish to thank Mr. Yan Lu, Yulin Zheng and Hongqi Chen of Tibet Bureau of Geology and Exploration for their great help in field work. Finally, the authors thank professor Watanabe and professor Imai for their careful review and useful suggestions, which resulted in improvements to the early version of this article.

## References

Cathelineau, M. (1988) Cation Site occupancy in chlorites and illites as a function of temperature. Clay Mineral., 23, 471–485.

Grant, J. A. (1986) The isocon diagram—a simple solution to Gresens' equation for metasomatic alteration. Econ. Geol., 81, 1976–1982.

Hezarkhani, A. (2002) Mass changes during hydrothermal alteration/mineralization in a porphyry copper deposit, eastern Sungun, northwestern Iran. J. Asian Earth Sci., 20, 567–588.

Hou, Z. Q., Qu, X. M., Wang, S. X., Gao, Y. F., Du, A. D. and Huang, W. (2003) The Re-Os age of molybdenites from Gangdese porphyry copper deposits belt, Xizang plateau: Mineralization age and application of dynamic setting. Sci. China Ser. D, 33, 609–618.

Huang, J. Q. and Chen, B. W. (1987) Geological Evolution of Tethys Sea around China and its Adjacent Areas. Geological Publishing House, Beijing, 78p.

Idrus, A., Kolb, J. and Meyer, E. M. (2009) Mineralogy, lithogeochemistry and elemental mass balance of the hydrothermal alteration associated with the gold-rich Batu Hijau porphyry copper deposits, Sumbawa Island, Indonesia. Resour. Geol., 59, 215–230.

Jowett, E. C. (1991) Fitting iron and magnesium into the hydrothermal chlorite geothermometer. GAC/MAC/SEG Joint Annual Meeting (Toronto) Abstract, A62.

Kapp, P., Murphy, M. A., Yin, A., Harrison, M. T., Ding, L. and Guo, J. H. (2003) Mesozoic and Cenozoic tectonic evolution of the Shiquanhe area of western Tibet. Tectonics, 22, 1029, doi:10.1029/2001TC001332, 2003.

Li, G. M., Li, J. X., Qin, K. Z., Zhang, T. P. and Xiao, B. (2007a) High temperature, salinity and strong oxidation ore-forming fluid at Duobuza gold-rich porphyry copper in the Bangonghu tectonic belt, Tibet: Evidence from fluid inclusions study. Acta Petrol. Sin., 23, 935–952 (in Chinese with English abstract).

Li, G. M., Qin, K. Z., Ding, K. S., Liu, T. B., Li, J. X., Wang, S. H., Jiang, S. Y. and Zhang, X. C. (2006) Geology, Ar-Ar age and mineral assemblage of Eocene skarn Cu-Au ± Mo deposits in the southeastern Gangdese arc, Southern Tibet: Implications for deep exploration. Resour. Geol., 56, 315–336.

Li, J. X., Li, G. M., Qin, K. Z. and Xiao, B. (2008) Geochemistry of porphyries and volcanic rocks and ore-forming geochronology of Duobuza gold-rich porphyry copper deposit in Bangonghu belt, Tibet: Constraints on metallogenetic tectonic settings. Acta Petrol. Sin., 24, 531–543 (in Chinese with English abstract).

Li, J. X., Li, G. M., Qin, K. Z. and Xiao, B. (2011a) High temperature primary magmatic fluid directly exsolved from magma at Duobuza gold-rich porphyry copper deposit, Northern Tibet. Geofluids, 11, 134–143.

Li, J. X., Li, G. M., Qin, K. Z., Xiao, B., Chen, L. and Zhao, J. X. (2012) Mineralogy and mineral chemistry of the Cretaceous Duolong gold-rich porphyry copper deposit in the Bangongco arc, Northern Tibet. Resour. Geol., 62, 19–41.

Li, J. X., Li, G. M., Qin, K. Z., Xiao, B., Zhao, J. X. and Chen, L. (2011b) Magma-hydrothermal evolution of the Cretaceous Duolong gold-rich porphyry copper deposit in the Bangongco metallogenetic belt, Tibet: evidence from U-Pb and $^{40}Ar/^{39}Ar$ geochronology. J. Asian Earth Sci., 41, 525–536.

Li, J. X., Qin, K. Z., Li, G. M. and Yang, L. K. (2007b) K-Ar and $^{40}Ar/^{39}Ar$ age dating of Nimu porphyry copper orefield in Central Gangdese: Constrains on magmatic-hydrothermal evolution and ore-forming tectonic setting. Acta Petrol. Sin., 23, 953–966 (in Chinese with English abstract).

Liao, L. G., Cao, S. H., Xiao, Y. B., Ouyang, K. G., Hu, Z. R. and Feng, G. S. (2005) The delineation and significance of the continental margin volcanic magmatic arc zone in the northern part of the Bangong Nujiang suture zone. Sedim. Geol. Tethyan Geol., 25, 163–170 (in Chinese).

No.5 Geological Team, Tibet Bureau of Geology and Exploration (TBGE) (2003) Geological reconnaissance report of the Duobuza ore district (unpublished).

Qin, K. Z., Li, G. M., Zhang, Q., Li, J. X., Maio, Y., Xiao, B., Zhang, T. P., Duo, J., Li, J. G. and Lu, Y. (2006) Metallogenic conditions and possible occurrences for epithermal gold mineralizations in Gangdese and Bangonghu Belts, Tibet—In view of porphyry-epithermal Cu-Au metallogenetic systematics. Proceedings of 8th State Mineral Deposit Conference, Geological Publishing House, Beijing. 660–670 (in Chinese).

Qin, K. Z., Tosdal, R., Li, G. M., Zhang, Q. and Li, J. L. (2005) Formation of the Miocene porphyry Cu (-Mo-Au) deposits in the Gangdese arc, southern Tibet, in a transitional tectonic setting. In Zhao, C. and Guo, B. (eds.) Mineral Deposit Research: Meeting the Global Challenge, Vol. 3. China and Publishing House, Beijing, 44–47.

Rui, Z. Y., Hou, Z. Q., Qu, X. M., Zhang, L. S., Wang, L. S. and Liu, Y. L. (2003) Metallogenetic epoch of Gangdese porphyry copper belt and uplift of Qinghai- Tibet Plateau. Miner. Deposit., 22, 217–224 (in Chinese with English abstract).

She, H. Q., Li, J. W., Ma, D. F., Li, G. M., Zhang, D. Q., Feng, C. Y., Qu, W. J. and Pan, G. T. (2009) Molybdenite Re-Os and SHRIMP zircon U-Pb dating of Duobuza porphyry copper deposit in Tibet and its geological implications. Miner. Deposit., 28, 737–746 (in Chinese with English abstract).

Shi, R. D. (2007) SHRIMP dating of the Bangong Lake SSZ-type ophiolite: Constraints on the closure time of ocean in the Bangong Lake-Nujiang River, northwestern Tibet. Chin. Phys. Lett., 52, 936–941.

Sillitoe, R. H. (2000) Gold-rich porphyry copper deposits: Descriptive and genetic models and their role in exploration and discovery. Rev. Econ. Geol., 13, 315–345.

Ulrich, T. and Heinrich, C. A. (2001) Geology and Alteration Geochemistry of the Porphyry Cu-Au Deposit at Bajo de la Alumbrera, Argentina. Econ. Geol., 96, 1719–1742.

Xiao, B., Li, G. M., Qin, K. Z., Li, J. X., Zhao, J. X., Liu, X. B., Xia, D. X., Wu, X. B. and Peng, Z. W. (2008) The magmatic intrusion center and mineralization center of Qulong giant porphyry Cu-Mo deposit, Tibet: evidence from fissure-veinlet and mineralization intensity. Miner. Deposit., 27, 200–208 (in Chinese with English abstract).

Xin, H. B., Qu, X. M., Wang, R. J., Liu, H. F., Zhao, Y. Y. and Huang, W. (2009) Geochemistry and Pb-Sr-Nd isotopic features of ore-bearing porphyries in Bangong Lake porphyry copper belt, western Tibet. Miner. Deposit., 28, 785–792 (in Chinese with English abstract).